Performances of BLDCM Drive System for Treadmill Application

Jin-Woo Ahn* and Dong-Hee Lee**

Abstract - In this paper, a BLDC motor and its controller are developed for treadmill application. Motor size and structure are restricted in the design stage due to the limited and enclosed space of the treadmill. The shape of the rotor magnet is analyzed using FEM with restricted design conditions. Manufacturing, cost and performance are also considered. A biomechanical analysis of human locomotion with the change of velocity is considered in the design of the controller.
For stable operation of the treadmill, current and temperature are to be detected by the DSP controller. The prototype BLDCM and its controller are tested to verify its performances.

Keywords: brushless DC motor, tread mill, DSP

1. Introduction

A brushless DC and its controller are developed for treadmill application. The BLDC motor has high efficiency and high power density characteristics [1-3]. In the restricted design conditions of 24 slot and stator structure, proper magnet arc and length of magnet end are investigated for high output torque and low cogging torque. The drive system is placed in the enclosed driving room of the treadmill, and motor size and stator structure are restricted in the design stage. To determine suitable design parameters, a simple numerical and FEM analysis are implemented. The shape of the permanent magnet is investigated for fabrication problems and motor performance. In addition, tuned gains from evolution strategy are used for performance improvement with biomechanical analysis of human motion.

2. Design and Analysis of BLDCM

2.1 Design Parameters

In this paper, a 2.5[HP]/220V BLDCM for treadmill application is designed. Fig. 1 shows the configuration of the treadmill motor. For stable operation, both a double pulley and a belt are adopted in the application, and the operating speed is determined by the pulley ratio and motor speed.

In order to produce sufficient output torque and high efficiency drive with the given restricted dimension shape of the permanent magnet, winding data are designed as a result of FEM analysis. Table 1 displays the design specifications of the prototype motor.

* Dept. of ECE, Kyungsung University, Busan, Korea. (jwahn@star.ks.ac.kr)
** OTIS-LG, Korea. (dhlee5@hanmail.net)
Received: April 18, 2003 ; Accepted: August 22, 2003

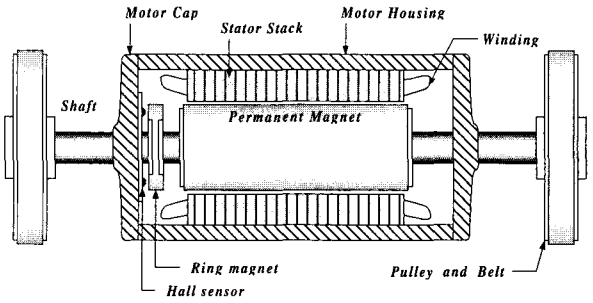

Fig. 1 Configurations of treadmill motor drive

Table 1 The specifications of BLDCM

Rated Power	2.5 [HP]	Phase Number	3
Rated Voltage	220 [V]	Connection	Y
Rated Speed	3000 [rpm]	Pole Number	4
Stack Length	140 [mm]	Air Gap	1.0 [mm]
Slot Number	24	Slot Depth	12 [mm]
Pole Arc	180 [deg.]	Magnet Depth	13 [mm]
Turn Number	25	Outer Radius	59 [mm]

A three-phase BLDC motor is generally designed so that the flat top of the phase back-EMF waveform is just over 120° wide. Each phase is supplied with a current waveform consisting of blocks with a constant current of 120° wide. During each 120° period, the electromagnetic power conversion can be calculated as follow.

$$e_a i_a + e_b i_b + e_c i_c = T_e \omega_m \tag{1}$$

where, T_e: electromagnetic torque, ω_m: mechanical rotor speed

In (1), e_a is back-EMF of a phase, and i_a is phase current. If the EMF and current waveforms are sufficiently flat dur-

ing this period, and the speed is essentially constant, the electromagnetic torque is also constant. In general, electromagnetic torque and mechanical rotor speed are determined by design requirements.

The EMF can be calculated from the air-gap flux distribution. If B_g is the average flux-density over one pole-pitch, the air-gap flux Φ_g is identified as follow.

$$\Phi_g = \int_0^{\pi/p} B(\theta) r \theta L_{stk} = B_g \frac{\pi D L_{stk}}{2p} \quad (2)$$

where, r is the stator bore radius, D is the stator bore diameter, L_{stk} is the stack length, and p is the number of pole-pairs.

The peak EMF per phase can be written as follow.

$$E_a = \omega_m \cdot \frac{2p}{\pi} \cdot T_{ph} \Phi_g \quad (3)$$

where, T_{ph} is the number of turns in series per phase. The air-gap flux is supplied by a permanent magnet attached to the rotor yoke. For the selection of magnet material, cost and environmental configuration must be considered. Recently, rare-earth magnetic material is widely used for high flux density, but the cost is still excessive and demagnetization is serious in high temperatures. In treadmill application, driving room is enclosed and cooling conditions are poor.

In this paper, the permanent magnet on the rotor is made out of ferrite material, and has a flux density of 0.405 [Tesla]. The ferrite magnetic material has a low temperature coefficient, and the manufacturing cost is lower than that of rare-earth magnetic material. In order to protect the ferrite from mechanical damage, a thin fibrous can is wrapped on the permanent magnet of the rotor structure. In consideration of operating speed, the number of poles and attached type are determined as a 4-pole structure and surface mounted type.

Under restricted design conditions, rotor pole arc is determined as 180 electrical degrees for the highest output power. However, the shape of the attached permanent magnet affects the output characteristics of the motor. The shape and depth of the rotor magnet are determined by fabrication and demagnetization problems. Since permanent magnets with complex shapes increase manufacturing costs, simply cutting the magnet end is considered a more economical means for improving motor performance. In order to reduce cogging torque and increase output torque, the length of magnet end is investigated by FEM analysis.

Fig. 2 and Fig. 3 show the back EMF waveform and output characteristics according to length of magnet end in circumference magnet shape.

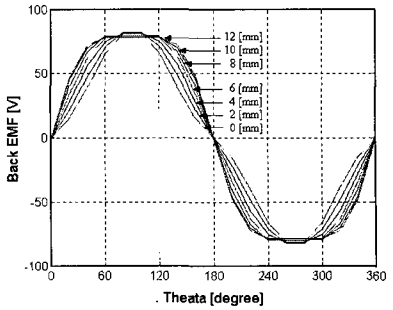

Fig. 2 Back EMF waveform according to the length of magnet end

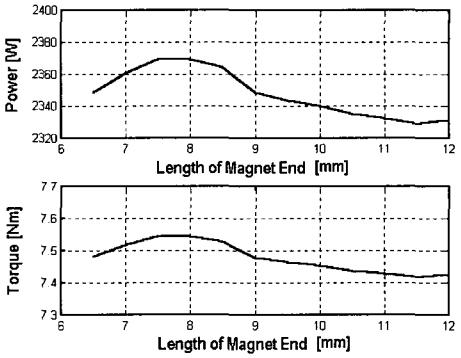

(a) output power and torque

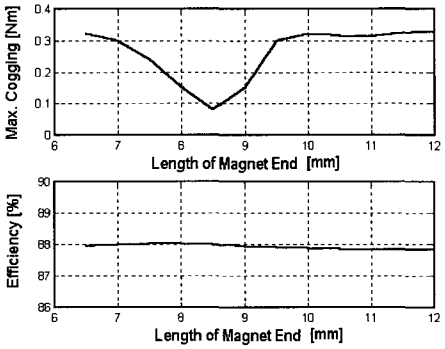

(b) maximum cogging torque and efficiency

Fig. 3 Characteristics analysis according to the length of magnet end

In Fig. 2 and Fig. 3, back EMF of stator winding depends on both winding method and permanent magnet shape. With FEM analysis, output power and torque are the highest at 8[mm] of the magnet end, and maximum cogging torque is minimized at 8.5[mm] of the magnet end. Since the treadmill inertia is very large, the effect of cogging torque can be reduced. The length of permanent magnet end is determined as 8[mm] from the view of output torque.

The practical winding is selected according to current density of winding and slot fill factor. Calculated wire diameter is 1.3[mm], but four strands of parallel windings are used as a winding for the manufacture.

2.2 Analysis of Dynamic Characteristics

A numerical analysis is used for verification of prototype motor design. Fig. 4 shows a simple block diagram of nonlinear magnetic circuit representing the MMF drops associated with one air-gap. The permanent magnet is represented by a Thevenin's equivalent circuit comprising the MMF, F_{ma} and the reluctance, R_{m0} in Fig. 4. The flux densities in the yoke and teeth sections are calculated from their permeance area, and the associated MMF drops are obtained using the nonlinear B-H curve of the steel. A simple equivalent magnetic circuit is solved iteratively. The basic result of the nonlinear magnetic circuit calculation is air-gap flux and the average flux density over the magnet pole arc.

With a simple estimation of the air-gap flux Φ_g, the permeance in an equivalent nonlinear model can be calculated as follow.

$$P_{m0} = \mu_r \mu_0 \frac{A_M}{L_M} = \mu_r \mu_0 \frac{\beta_M}{2} \frac{r_M L_{STK}}{L_M} \tag{4}$$

where, β_M is the pole-arc of the magnet in mechanical radians, A_M is the magnet half-pole area, L_{STK} is the stack length, and L_M is the magnet length in the direction of magnetization. The radius r_M is the effective radius of the magnet. Similarly the air-gap reluctance is

$$\Re_g = \frac{g}{\mu_0 A_g} \tag{5}$$

where A_g is the air-gap area.

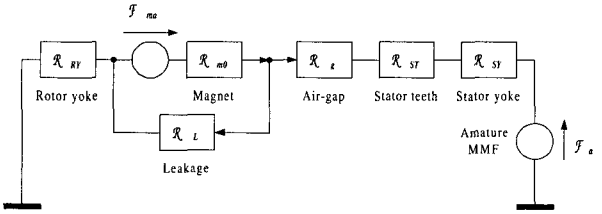

Fig. 4 A simple block diagram of nonlinear magnetic circuit

Total magnetizing force in the magnet is calculated as:

$$H_m = \frac{\left(F_g + F_{SY} + F_{RY} + F_{ST}\right)}{L_M} \tag{6}$$

Table 2 shows the general output characteristics of designed motor in time-step method when the motor is controlled by 120° commutation and current chopping. From the analysis results, requirement performance is satisfied by the prototype motor.

Table 2 Output characteristics of the designed motor

Output torque	7.532 [Nm]	Output power	2,366 [W]
Copper loss	304 [W]	Iron loss	14 [W]
Total loss	318 [W]	Efficiency	88 [%]
Current density	8.1 [A/mm2]	RMS current	10 [A]

Fig. 5 shows the speed-torque curve. From the numerical analysis, required conditions are satisfied by the designed prototype motor.

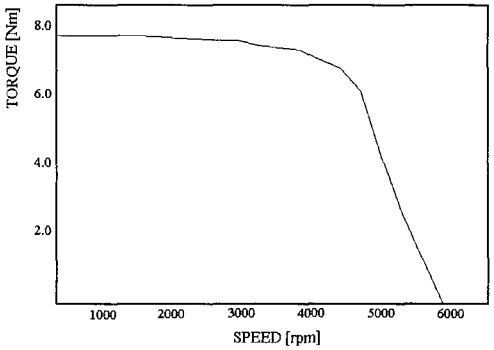

Fig. 5 Speed-torque curve

The main controller is designed by TMS320F241 of Texas Instruments. A basic switching pattern is generated by a hall sensor and disk type ring magnet on the moving shaft. The three Hall Effect sensors provide three overlapping signals giving a 60° wide position range. The three signals can be wired to the DSP input Capture pins, thus speed information is available by measuring the time interval between two input Captures. The time interval is automatically stored by the DSP into a specific register at each input Capture. In this paper, Timer 2 of DSP is selected as the time base for the capture unit and it is set in continuous up-count mode. The driver uses the 120° commutation method, and the controller is to have only one current at a time in the motor. Consequently, it is unnecessary to position a current sensor on each phase of the motor. One sensor placed in the line inverter input makes it possible to control the current of each phase. The current information is also used to protect over-current.

Fig. 6 shows sensor signals and switching patterns.

A PWM technique and P.I. control method are used for speed control of a treadmill. At the starting and operating, smooth running is required for user safety. Gains of speed controller are tuned by evolution strategy as considerations of user weight and command speed.

Fig. 7 shows the block diagram of speed controller using TMS320F241. The actual speed of the motor is calculated by a CAPTURE module with timer2 in DSP.

The speed feedback is derived from the output signals of

the position sensor. From the position signals, the time interval between 60 electrical degrees can be detected. The speed of the motor can be calculated as follow.

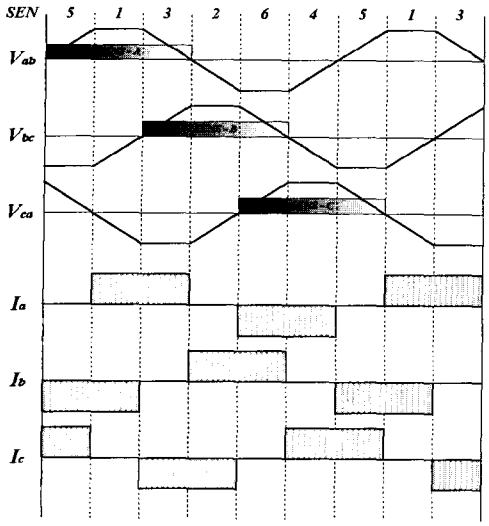

Fig. 6 Sensor signals and phase current according to switching pattern

$$\omega_r = \Delta\theta / \Delta t \tag{7}$$

where, θ is the electrical angle at which it is possible to obtain the speed from the computed elapsed time between two captures. Between two commutation signals the angle variation is constant as the Hall Effect sensors are fixed relative to the motor, so speed sensing is reduced to a simple division. And the speed control is implemented by the duty cycle of each commutated power switch as follows.

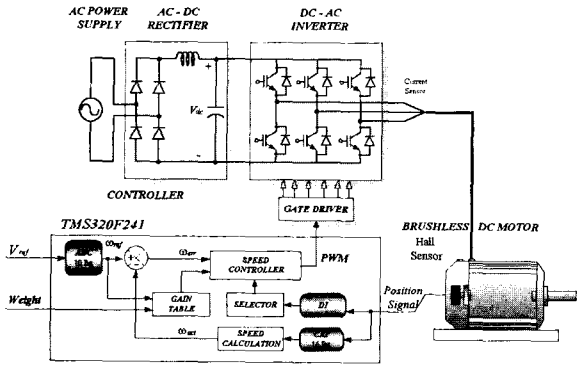

Fig. 7 The global block diagram of the controller

$$\Delta\omega = \omega_{ref} - \omega_r \tag{8}$$

$$T_{on} = K_P(\omega_r, W_T) \cdot \Delta\omega + K_I(\omega_r, W_T) \cdot \int \Delta\omega \cdot dt \tag{9}$$

where, T_{on} denotes turn-on time of PWM period. $K_P(\omega_r, W_T)$ and $K_I(\omega_r, W_T)$ are the learned gains according to motor speed (ω_r) and user weight (W_T), respectively.

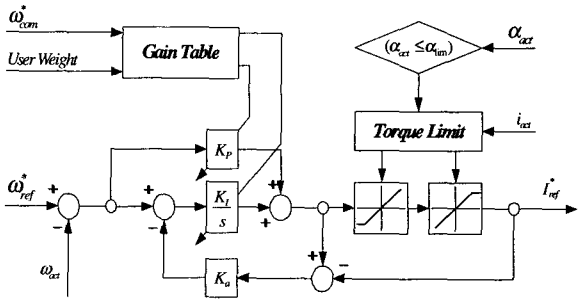

Fig. 8 Block diagram of speed controller

The control gains are stored in the memory table. Over current is detected by current sensor L16P025 of the Tamura Company. The output signal of the current sensor and over current limit reference are compared to protect over current of the drive. Fig. 8 shows speed controller which uses PI controller. The gain is calculated using weight of the user and applies an anti-windup integrator to have a stable transient response.

3. Experimental Results

Fig. 9 shows the housing and rotor structure of the prototype motor. For effective cooling of the stator, aluminum housing is used.

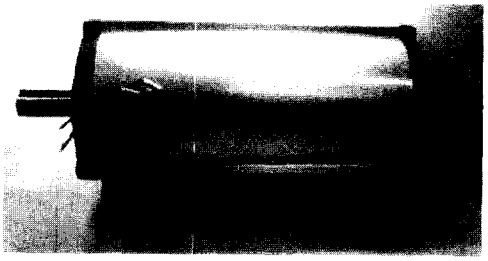

(a) prototype motor

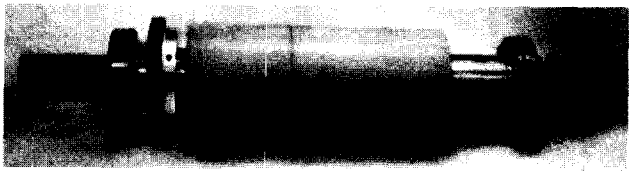

(b) rotor with ring magnet

Fig. 9 Prototype motor and rotor with ring magnet

Fig. 10 shows the starting characteristics at rated speed conditions with 1.5 [kW] load. The actual speed is reached at 3000 [rpm] in 150[ms], and the current is stable after starting.

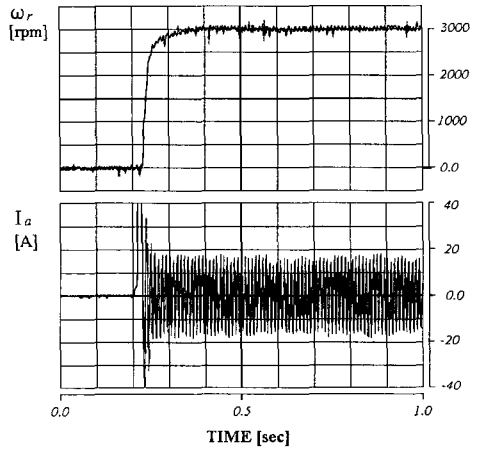

Fig. 10 Starting characteristics at rated speed condition

Fig. 11 shows speed response and current waveform at 500[rpm] and 3000[rpm] of reference speed, respectively. In a wide operating region, experimental results show stable speed responses at a sudden load disturbance.

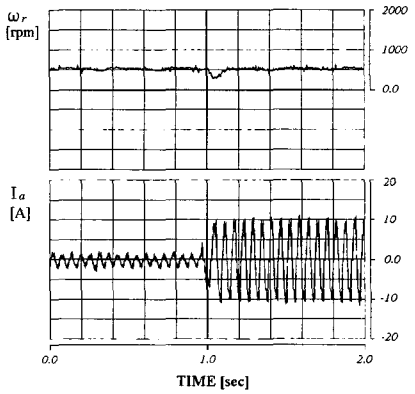

(a) load applied

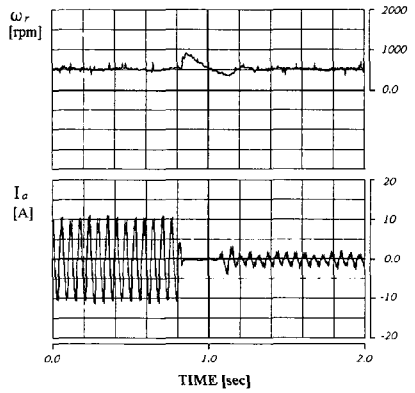

(b) load removed

Fig. 11 Speed response with load disturbance at 500[rpm]

Fig. 12 and Fig. 13 illustrate performance of the prototype treadmill. The treadmill responds well when it is used for running. The tests are executed using an 85[Kg] adult male.

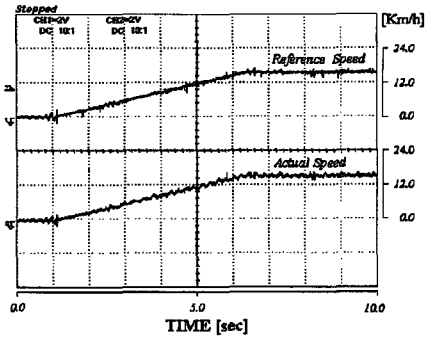

(a) Speed tracking

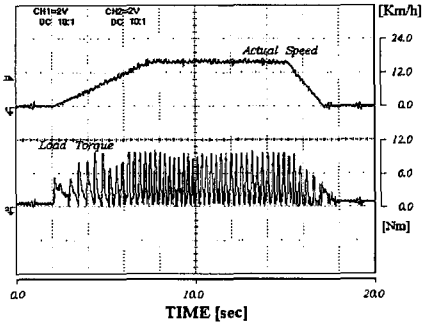

(b) Speed and torque

Fig. 12 Acceleration and deceleration response

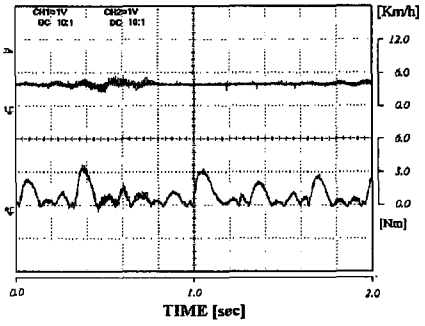

(a) walking (4Km/h)

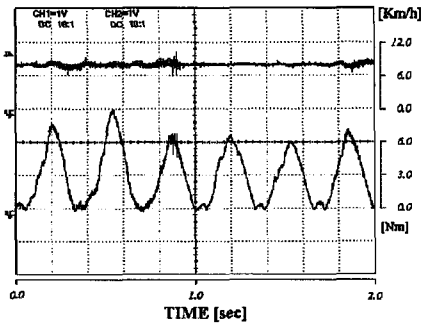

(b) running (7Km/h)

Fig. 13 Walking and running response

Fig. 14 shows the efficiency and torque characteristics. The measured efficiency is 86.8[%] at rated load, which is equal to the analyzed result.

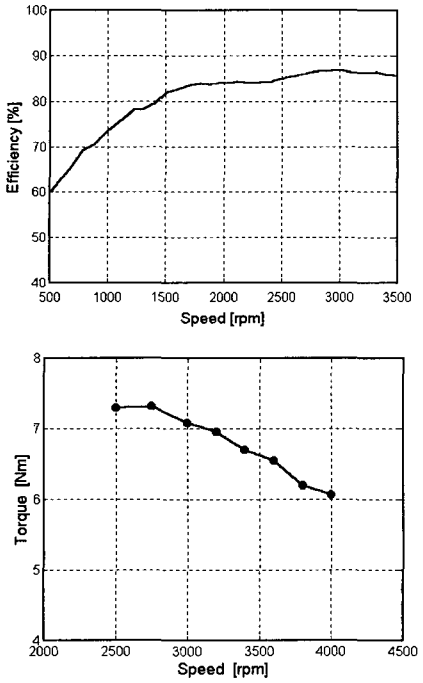

Fig. 14 Efficiency and torque of the prototype motor

5. Conclusion

A BLDCM and DSP controller are designed for commercial treadmill application. The prototype motor is analyzed by both a numerical and FEM analysis. Analyzed results indicate that the performances satisfy the requirements. At restricted stator core, the shape of the permanent magnet is analyzed by FEM analysis, and the shape is selected considering output and cogging torque with restricted conditions.

For stable operation, controller gains are tuned by evolution strategy according to user weight and reference speed. Over-current and overheating protection circuits are applied for robust drive. Experimental results show stable operating characteristics in a wide speed range.

References

[1] P. Vas, *Sensorless Vector and Direct Torque Control*, Oxford Univ. Press, 1998.

[2] K. Rajashekara, A. Kawamura and K. Matsuse, *Sensorless Control of AC Motor Drives*, IEEE Press, 1996.

[3] Peter Vas, *Vector Control of AC Machines*, CLARENDON Press, 1990.

[4] A. T. Morgan, *General Theory of Electrical Machines*, Heyden & Son Ltd. 1979.

[5] S. A. Nasar, I. Bolder and L. E. Unnewehr, *Permanent Magnet, Reluctance, and Self Synchronous Motors*, CRC Press, 1993.

[6] J.W. Ahn et al, "The Optimal Link Voltage of Digitally Implemented SVPWM Inverter for Current Ripple minimization," Proc. of ICEE 2002, pp. 821-825, 2002

Jin-Woo Ahn

He was born in Busan, Korea, in 1958. He received his B.S., M.S., and Ph.D. degrees in Electrical Engineering from Pusan National University, Busan, Korea, in 1984, 1986, and 1992, respectively.

He has been with Kyungsung University, Busan, Korea, as a Professor in the Department of Electrical and Computer Engineering since 1992. He was a Visiting Professor in the Dept. of EE, UW-Madison, USA from 1998 to 1999. He is the author of five books including SRM and the author of more than 100 papers. His current research interests are Motor Drive System and Electric Vehicle Drive.

Dr. Ahn is a life member of the Korean Institute of Electrical Engineers, a member of the Korean Institute of Power Electronics and a senior member of IEEE.

Tel: +82-51-620-4773

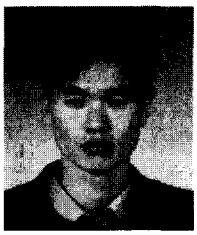

Dong-Hee Lee

He was born on Nov. 11, 1970 and received his B.S, M.E, and Ph.D. degrees in Electrical Engineering at Pusan National University. His major research field is the motor drive system and micro-processor applications. He is a member of KIEE and is currently working as a Senior Researcher at OTIS-LG.

Tel: +82-51-522-1503